

# Effects of Incident Light Modes and Non-Uniform Sensing Layers on Fiber-Optic Sensors Based on Surface Plasmon Resonance

Yuzhi Chen<sup>1,2,4</sup> · Xuejin Li<sup>1,2,4</sup> · Huasheng Zhou<sup>2,4,5</sup> · Qingli Xie<sup>2,3,4</sup> · Xueming Hong<sup>2,4,5</sup> · Youfu Geng<sup>2,4,5</sup>

Received: 27 April 2016 / Accepted: 14 June 2016 / Published online: 30 June 2016  
© Springer Science+Business Media New York 2016

**Abstract** There are two important factors, which are easily neglected, restricting the sensing performance of fiber-optic surface plasmon resonance (SPR) sensors. These are the selection of incident light modes and the uneven distribution of the sensing layer. In this paper, a fiber-optic SPR sensor model with a non-uniform sensing layer is first proposed. We use fiber-optic SPR sensor models with uniform and non-uniform sensing layers to study the impact of incident light modes and sensing layer non-uniformities on their sensing performances, respectively. In the case of a uniform sensing layer, the contributions of different single incident light modes are investigated and the optimal incident multimode form is selected as  $1.41 \sim \pi/2$ ; the optimal thickness of the sensing layer is selected as 65 nm. In the case of a non-uniform sensing layer, the non-uniformity of the sensing layer has little effect on the sensing performances when the length of the sensing region is 10 mm. However, the length of the sensing region has an obvious effect on the sensing performances.

**Keywords** Fiber-optic sensor · Surface plasmon resonance · Non-uniform sensing layer · Incident light mode

## Introduction

Surface plasmon resonance (SPR) describes the resonant oscillation of conduction electrons at the interface between a metal and a dielectric [1, 2]. Owing to its high sensitivity to the refractive index (RI), many chemical and biological studies have been reported by using SPR sensors. For example, the detection of pharmaceutical compounds [3], the study on biomolecular specificity [4], and the real-time measurement of biochemical interactions [5]. However, the traditional SPR sensors based on a prism can only be used in the laboratory due to its large volume and complexity. In 1993, a flexible and miniaturized structure of an SPR sensor, which integrated the sensor in an optical fiber, was proposed by Jorgenson and Yee [6]. On account of its unique advantages, such as its compactness, in situ sensing capability, and in vivo detecting adaptability [7], the fiber-optic SPR sensor attracts more and more attention from researchers.

Recently, researchers have made efforts to improve the performances of fiber-optic SPR sensors. Yuan et al. theoretically investigate the effects of the geometric parameters on the performance of a SPR-based optical fiber tip sensor, and their results show that an increase of the tip angle may lead to a small increase in its sensitivity, but also broadens the resonance dip and decreases the signal-to-noise ratio [1]. Sharma et al. propose a fiber-optic SPR sensor with ITO-Au bilayers. Its best sensitivity is about 1929 nm/RIU [8]. Liu et al. fabricate an SPR sensor on a twin-core fiber. The sensor uses a single-mode beam to excite surface plasmons and obtains a high RI sensitivity of 5213 nm/RIU. It also reduces the mode noise effectively [9]. Nayak et al. report on an optical fiber

✉ Xuejin Li  
lixuejin@szu.edu.cn

<sup>1</sup> College of Optoelectronic Engineering, Shenzhen University, Shenzhen 518060, P. R. China  
<sup>2</sup> Shenzhen Key Laboratory of Sensor Technology, Shenzhen 518060, P. R. China  
<sup>3</sup> College of Electronic Science and Technology, Shenzhen University, Shenzhen 518060, P. R. China  
<sup>4</sup> Shenzhen Engineering Laboratory for Optical Fiber Sensors and Networks, Shenzhen 518060, P. R. China  
<sup>5</sup> College of Physics Science and Technology, Shenzhen University, Shenzhen 518060, P. R. China

based localized SPR sensor by using graphene oxide encapsulated Au nanoparticles. Its resolution is obtained to be  $8.7 \times 10^{-5}$  RIU in sucrose measurements [10]. However, researchers neglect some essential factors which restrict the sensing performances of fiber-optic SPR sensor. There are two important factors: the selection of incident light modes and the uneven distribution of the sensing layer.

At the beginning of our investigation, we use a fiber-optic SPR sensor model with a uniform sensing layer to study the contributions of different single incident light modes to the sensing performances and then select the optimal incident multimode form and thickness of sensing layer. On this basis, we propose a fiber-optic SPR sensor model with a non-uniform sensing layer which can be set to satisfy different coating conditions and study the influence of non-uniform sensing layers on the sensor. To our knowledge, this presents the first investigation on the effect of non-uniform sensing layers on fiber-optic SPR sensors. Our results show that the non-uniformity of the sensing layer has little effect on the sensing performances when the length of the sensing region is 10 mm. However, the length of the sensing region has an obvious effect on the sensing performances in the case of a non-uniform sensing layer.

## Models and Method

The transmission type of a fiber-optic SPR sensor, which is shown in Fig. 1, works with wavelength modulation, and a three-layer model is used for description. The first layer is the 600- $\mu\text{m}$ -diameter silica fiber core whose RI varies with wavelength according to the Sellmeier dispersion relation:

$$n_c(\lambda) = \sqrt{1 + \frac{a_1 \lambda^2}{\lambda^2 - b_1^2} + \frac{a_2 \lambda^2}{\lambda^2 - b_2^2} + \frac{a_3 \lambda^2}{\lambda^2 - b_3^2}} \quad (1)$$

where  $\lambda$  is the wavelength of incident light in micrometer,  $a_1$ ,  $a_2$ ,  $a_3$ ,  $b_1$ ,  $b_2$ , and  $b_3$  are Sellmeier coefficients. The values are

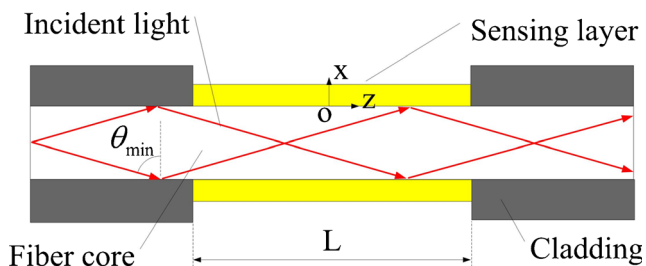


**Fig. 1** Model of a fiber-optic SPR sensor with a uniform sensing layer

given as:  $a_1 = 0.6961663$ ,  $a_2 = 0.4079426$ ,  $a_3 = 0.8974794$ ,  $b_1 = 0.0684043 \mu\text{m}$ ,  $b_2 = 0.1162414 \mu\text{m}$ , and  $b_3 = 9.896161 \mu\text{m}$  [11], respectively.

The second layer is the metal sensing layer. Here, we choose silver (Ag) as the material of the sensing layer for its highest sensitivity and resolution in SPR detection [12]. According to the Drude formula, the dielectric constant of any metal can be written as:

$$\varepsilon_m(\lambda) = \varepsilon_{mr} + i\varepsilon_{mi} = 1 - \frac{\lambda^2 \lambda_c}{\lambda_p^2 (\lambda_c + i\lambda)} \quad (2)$$

where  $\lambda_p$  and  $\lambda_c$  are the plasma wavelength and the collision wavelength of the metal, respectively.  $\lambda_p = 1.4541 \times 10^{-7} \text{ m}$  and  $\lambda_c = 1.7614 \times 10^{-5} \text{ m}$  for Ag [13]. The sensing layers of fiber-optic SPR sensors are always set to have a uniform distribution by other researches [14–16]. However, in actual operation, the sensing layers distribute unevenly both along circumferential and axial directions. The circumferential non-uniformity can be eliminated by inviting a rotating machine [17]. Nevertheless, the axial non-uniformity is more complicated and is studied and analyzed in detail in part “3.3.”

The third layer is the environmental media. In our research, the RI of the environmental media ranges from 1.33 to 1.38 with an interval of 0.01.

Light transmitted in the fiber core excites surface plasmons in the sensing region. Its transmission can be thus defined as a function of the light incident angle  $\theta$ , the wavelength  $\lambda$ , and the RI of the environmental media  $n_e$  [18, 19]:

$$I(\theta, \lambda, n_e) = \frac{1}{2} [R_p^N(\theta, \lambda, n_e) + R_s^N(\theta, \lambda, n_e)] \quad (3)$$

where  $N = d/L \tan\theta$  is the number of reflections with  $L$  being the length of the sensing region.  $R_p$  and  $R_s$  represent the reflection ratio of p- and s- polarized light, respectively.

The cascaded reflectance of the three-layer model can be described as [18]:

$$R = \left| \frac{r_{cm} + r_{me} \cdot \exp(2ik_{mz}T)}{1 + r_{cm} \cdot r_{me} \cdot \exp(2ik_{mz}T)} \right|^2 \quad (4)$$

Here, we let  $c$ ,  $m$ ,  $e$ , and  $z$  denote the fiber core, metal layer, environmental media, and direction along the  $z$ -axis, respectively.  $r_{cm}$  and  $r_{me}$  denote the reflection coefficients of the fiber-core/metal-layer and metal-layer/environmental-media

interfaces, and  $k_{mz}$  denotes the wave vector along the  $z$ -axis in the metal layer.  $T$  is the thickness of the uniform sensing layer.

Furthermore, the reflection coefficients of p- and s- polarized light are given as follows [18, 19]:

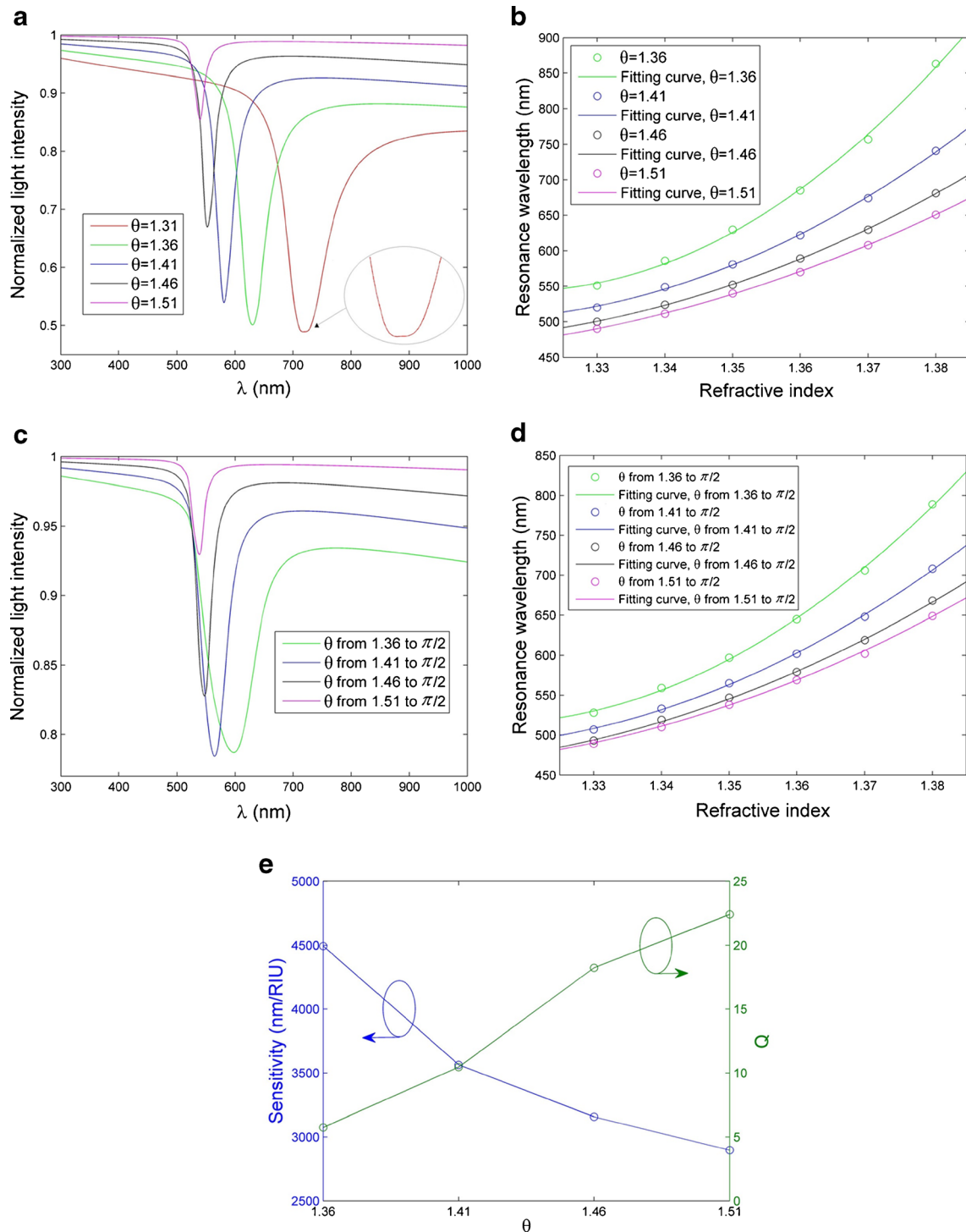


**Fig. 2** The normalized spectra, sensitivities and  $Q_s$  of fiber-optic SPR sensors with 65-nm uniform sensing layers. **a**, **b** are the comparisons of sensors with different single-mode incidences. **c**, **d** show the comparisons of sensors with different multimode incidences. The graphs on the left side display the resonance dips. The graphs on the right side show

sensitivities. The sensitivities and  $Q_s$  of sensors with different multimode incidences are detailedly described in **e**, while the blue curve presents sensitivity and the green curve is for  $Q_s$ . All the resonance dips, sensitivities, and  $Q_s$  are obtained when  $n_c = 1.35$

**Table 1** Sensing performance comparisons of fiber-optic SPR sensors with different single-mode incidences

$\theta$	1.36	1.41	1.46	1.51
$S$ (nm/RIU)	5251.10	3857.80	3266.10	2955.70
$Q$	10.5	14.90	19.71	25.71

**Table 2** Sensing performance comparisons of fiber-optic SPR sensors with different multimode incidences

$\theta$	1.36 ~ $\pi/2$	1.41 ~ $\pi/2$	1.46 ~ $\pi/2$	1.51 ~ $\pi/2$
$S$ (nm/RIU)	4493.90	3563.90	3156.90	2896.20
$Q$	5.74	10.46	18.23	22.42

$$r_{cm}^p = \frac{k_{cz}/n_c^2 - k_{mz}/\epsilon_m}{k_{cz}/n_c^2 + k_{mz}/\epsilon_m} \tag{5}$$

$$r_{me}^p = \frac{k_{mz}/\epsilon_m - k_{ez}/n_e^2}{k_{mz}/\epsilon_m + k_{ez}/n_e^2} \tag{6}$$

$$r_{cm}^s = \frac{k_{cz} - k_{mz}}{k_{cz} + k_{mz}} \tag{7}$$

$$r_{me}^s = \frac{k_{mz} - k_{ez}}{k_{mz} + k_{ez}} \tag{8}$$

In equations (5)–(8), all the wave vectors in different layers can be described as:

$$k_{iz} = \frac{2\pi}{\lambda} \cdot [n_i^2 - (n_c \sin\theta)^2]^{\frac{1}{2}} \tag{9}$$

where  $i$  can be replaced by  $c$ ,  $m$ , or  $e$ , and  $n_m^2 = \epsilon_m$ . When the resonance condition  $n_c \cdot 2\pi/\lambda \cdot \sin\theta = 2\pi/\lambda \cdot [\epsilon_m(\lambda) \cdot n_e^2/(\epsilon_m(\lambda) +$

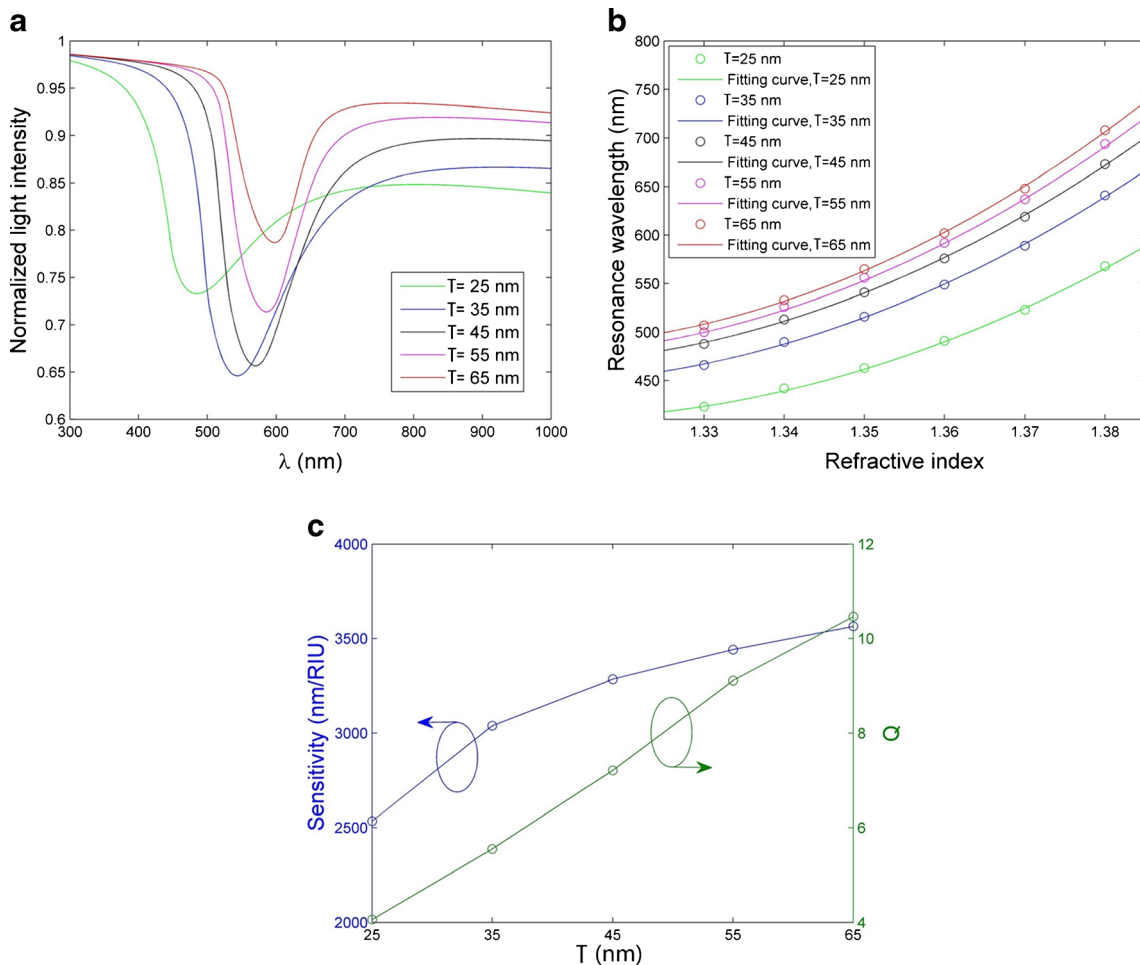


**Fig. 3** The normalized spectra, sensitivities and  $Q$ s of “1.41 ~  $\pi/2$ ” multimode incident fiber-optic SPR sensors with uniform sensing layers of different thicknesses. **a** The resonance dips; **b** the sensitivities; **c** the

detailed sensitivities and  $Q$ s, while the *blue curve* presents sensitivity and the *green curve* is for  $Q$ . All the resonance dips, sensitivities and  $Q$ s are obtained when  $n_e = 1.35$

**Table 3** Sensing performance comparisons of “1.41 ~ π/2” multimode incident fiber-optic SPR sensors with uniform sensing layers of different thicknesses

<i>T</i> (nm)	25	35	45	55	65
<i>S</i> (nm/RIU)	2533.70	3093.00	3284.90	3441.10	3563.90
<i>Q</i>	4.06	5.55	7.21	9.11	10.46

$n_e^2)^{1/2}$  is satisfied, the energy of incident light transfers to the input of a plasmonic wave and an absorption dip appears in the normalized transmission spectrum [20].

There are two important parameters used to describe the performances of SPR sensors. They are the sensitivity (*S*) and the quality factor of the resonance dip (*Q*), which can be written as [21]:

$$S = \frac{\delta\lambda_R}{\delta n_e} \tag{10}$$

$$Q = \frac{\lambda_R}{FWHM} \tag{11}$$

where  $\delta\lambda_R$  is the resonance wavelength ( $\lambda_R$ ) shift with the change of environmental media ( $\delta n_e$ ) and FWHM is the full width at half maximum of the resonance dip.

## Results and Discussion

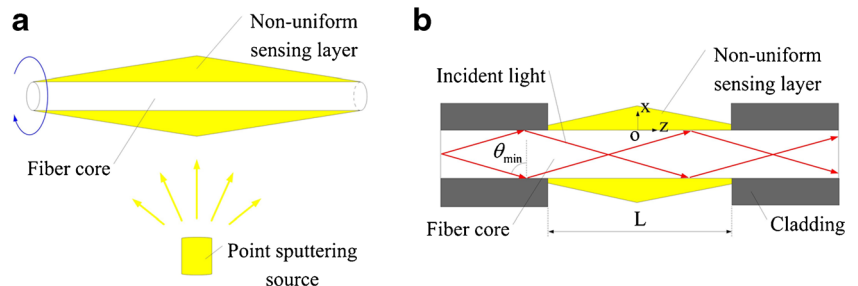
### Choice of the Incident Light Modes of the Fiber-Optic SPR Sensor with a Uniform Sensing Layer

In order to investigate the relationships between incident light modes and sensing performances, we assume that the sensor is fabricated from a silica fiber with a sensing region of  $L = 10$  mm and uniform sensing layer with thickness  $T = 65$  nm. We then control the incident light modes to calculate the corresponding performances, which are shown in Fig. 2.

In general, incident light, which satisfies the total reflection condition  $\theta > \theta_{cr} = \sin^{-1}(n_{cl}/n_c)$  (here,  $n_{cl}$  is the RI of fiber cladding), can transmit in the multimode fiber. However, the contributions of different single incident light modes (with different incident angle  $\theta$ s) to SPR are not clear yet. Thus, we first study the SPR excitation effects of different single-mode incidences, which are shown in the top row of Fig. 2. The single incident light modes between  $\theta_{cr}$  and  $\pi/2$ , which are set to  $\theta = 1.31, 1.36, 1.41, 1.46,$  and  $1.51$ , respectively, can excite SPR dips [as shown in Fig. 2a]. All the SPR dips, *S*, and *Q* discussed below were obtained for  $n_e = 1.35$ . One can see that the SPR dip shifts to longer wavelengths and the depth of the dip increases with decreasing  $\theta$ . However, the effective SPR excitation mode cannot reach  $\theta = 1.31$ , since the bottom of the “ $\theta = 1.31$ ” SPR dip becomes flat and the resonance point cannot be detected. The flat bottom of the SPR dip is mainly caused by penetration of the evanescent field of “ $\theta \leq 1.31$ ” high order incident modes through the Ag sensing layer, resulting in a light leak rather than a resonance absorption. From Fig. 2b and Table 1, we can see that *S* increases with decreasing  $\theta$  ( $\theta > 1.31$ ), while *Q* decreases.

Since the higher order (smaller  $\theta$ ) incident light mode increases *S*, but worsens *Q* and the multimode fiber supports incident light modes from  $\theta_{cr}$  to  $\pi/2$  (here,  $\theta_{cr}$  can be controlled by setting  $n_{cl}$ ), we further study the SPR excitation effects of different multimode incidences by changing  $\theta_{cr}$ , as described in the middle row of Fig. 2.  $\theta_{cr}$  is set to 1.36, 1.41, 1.46, and 1.51, respectively. In Fig. 2c, the SPR dip shifts to longer wavelength and the FWHM of the dip becomes wider with decreasing  $\theta_{cr}$ . The performances are illustrated in Fig. 2d and Table 2. In spite of more incident light modes involved in sensing (the energy distribution of different modes is taken into account, detailed in our prior study [16]), the high *S* is maintained, however, with *Q* decreasing strongly due to the obviously increasing FWHM. On the one hand, the decrease of  $\theta_{cr}$  increases the number of high order modes, which make contributions to increase *S*. On the other hand, the more incident light modes the more serious mode superposition is present, which leads to the broadening of the dip (reason for the deterioration of *Q*). Weighing up these two opposite trends,

**Fig. 4** Fiber-optic SPR sensor with a non-uniform sensing layer. **a** Reason for the non-uniform sensing layer; **b** sensor model



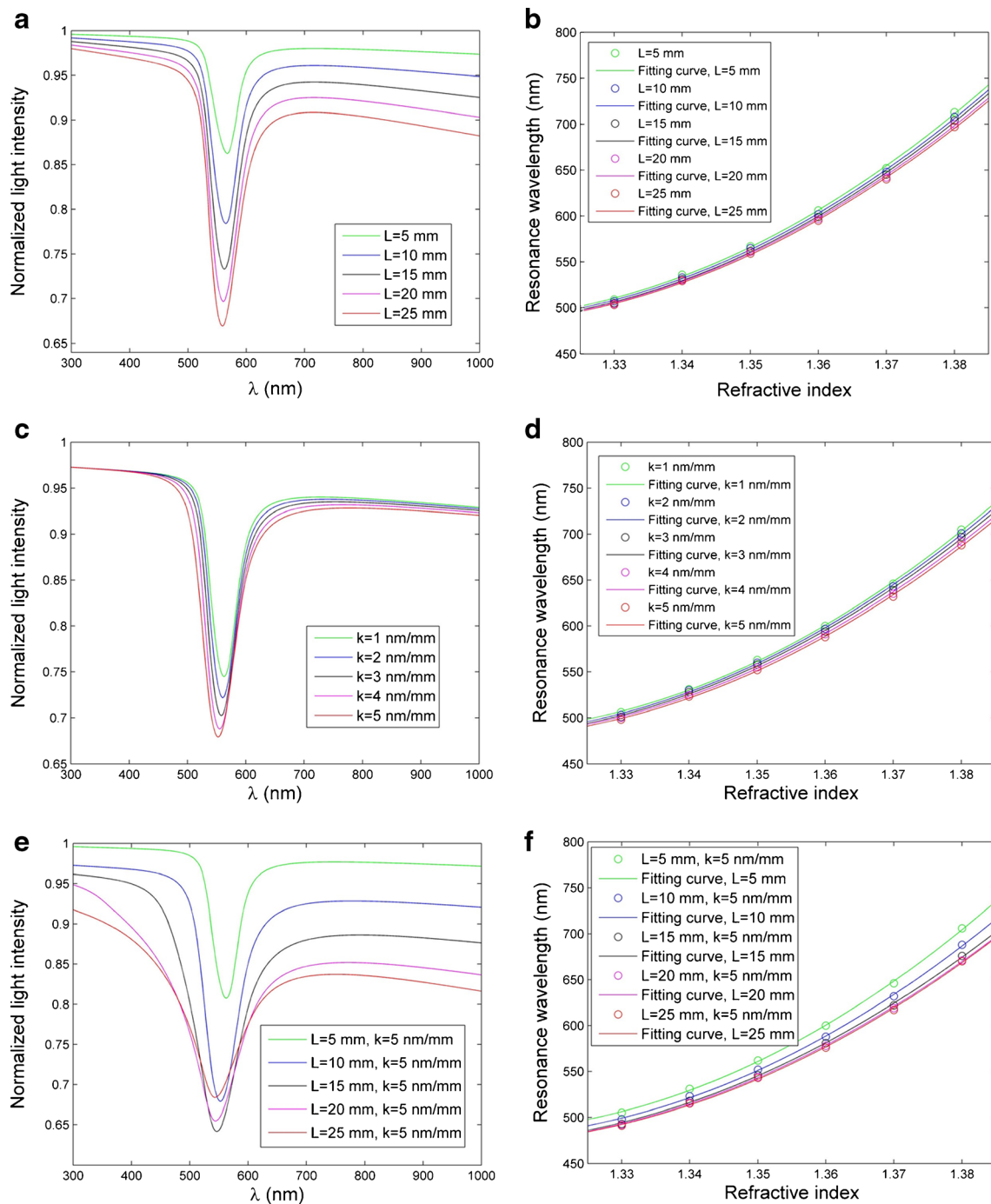


**Fig. 5** The normalized spectra and sensitivities of “ $1.41 \sim \pi/2$ ” multimode incident fiber-optic SPR sensors: **a**, **b** are the comparisons of sensors with 65-nm uniform sensing layers and different lengths of sensing regions; **c**, **d** show the comparisons of sensors with different non-uniform sensing layers and 10-mm lengths of sensing regions; **e**, **f**

describe the comparisons of sensors with “ $k = 5$  nm/mm” non-uniform sensing layers and different lengths of sensing regions. The graphs on the left side display the resonance dips. The graphs on the right side show sensitivities. All the resonance dips and sensitivities are obtained when  $n_e = 1.35$

we judge an optimal multimode form to be  $\theta = 1.41 \sim \pi/2$ . Thus, Fig. 2e shows us the optimal multimode form by crossing the decreasing  $S$  line and increasing  $Q$  line. The optimal multimode form is  $\theta = 1.41 \sim \pi/2$ .

### Choice of the Thickness of the Uniform Sensing Layer

After selecting the optimal multimode form  $\theta = 1.41 \sim \pi/2$ , we study the effect of sensing layer thickness on the sensing

**Table 4** Sensing performance comparisons of “1.41 ~ π/2” multimode incident fiber-optic SPR sensors with 65-nm uniform sensing layers and different lengths of sensing regions

<i>L</i> (mm)	5	10	15	20	25
<i>S</i> (nm/RIU)	3611.70	3563.90	3523.30	3471.70	3441.10
<i>Q</i>	11.81	10.46	9.69	9.05	8.47

performance. The sensing region is again set to  $L = 10$  mm. Figure 3a shows that the SPR dip has a red shift and the FWHM of the dip becomes narrower with increasing  $T$ , while the depth of the dip first increases and then decreases. Figures 3b, c and Table 3 describe  $S$  and  $Q$  of the sensor with different  $T$ . Since both  $S$  and  $Q$  are increasing with the increase of  $T$ , we choose our maximum  $T = 65$  nm for the optimal thickness of uniform sensing layer. It should be noted that the depth of dip cannot be too small; otherwise, it is easy to be submerged by noise. To our experience [20, 22], the SPR dip can be distinguished from noise when its depth is greater than 0.1. And all the depths of SPR dips in this paper are greater than 0.1.

**Effect of Different Non-Uniform Sensing Layers and Different Lengths of Sensing Regions on Sensing Performances**

In the actual operation, the sensing layers distribute unevenly both along circumferential and axial directions. By inviting a rotating machine [17], the circumferential non-uniformity can be eliminated. Nevertheless, the axial non-uniformity is more complicated. It is affected by, e.g., the coating method, the coating environment, the relative position and motion of optical fiber and coating material (when the optical fiber is coated), and the characteristics of coating material. Therefore, a fiber-optic SPR sensor model with non-uniform sensing layer along the axial direction is proposed. In this model, the distributions and non-uniformities of sensing layers can be set to satisfy different coating conditions. Taking the point sputtering source case as an example, as shown in Fig. 4a, the source

**Table 5** Sensing performance comparisons of “1.41 ~ π/2” multimode incident fiber-optic SPR sensors with different non-uniform sensing layers and 10-mm lengths of sensing regions

<i>k</i> (nm/mm)	1	2	3	4	5
<i>S</i> (nm/RIU)	3530.70	3511.80	3670.40	3402.90	3367.50
<i>Q</i>	10.23	9.66	9.15	8.41	7.67

**Table 6** Sensing performance comparisons of “1.41 ~ π/2” multimode incident fiber-optic SPR sensors with “ $k = 5$  nm/mm” non-uniform sensing layers and different lengths of sensing regions

<i>L</i> (mm)	5	10	15	20	25
<i>S</i> (nm/RIU)	3555.00	3367.50	3253.90	3194.30	3173.90
<i>Q</i>	10.81	7.67	5.35	4.06	3.96

is placed below the middle point of sensing region. From the middle to the two edges of the sensing region, the distance of source and sensing region becomes larger. After spin coating, the sensing layer thus has a thickness maximum in the center. To simplify the model, the thickness of the non-uniform sensing layer is assumed to be a linear variation from the middle to the two edges [see Fig. 4b]. Taking the middle of the sensing region as the origin  $O$ , the thickness of the non-uniform sensing layer varies along the  $z$ -axis, which can be expressed as:

$$T(z) = T_m - k \cdot |z| \tag{11}$$

where  $T_m$  and  $k$  denote the thickness at the center of the sensing layer and the linear change rate of the sensing layer thickness along the  $z$ -axis, respectively.

*Length of Sensing Region with Uniform Sensing Layer*

The top row of Fig. 5 and Table 4 illustrate the sensing performances of our fiber-optic SPR sensors with 65-nm uniform sensing layers and different  $L$ . The incident multimode form is set to  $\theta = 1.41 \sim \pi/2$ . The SPR dip basically remains in the same position, and its depth increases [see Fig. 5a], while  $S$  and  $Q$  slightly decrease with increasing  $L$  [see Fig. 5b and Table 4]. Thus, in the case of a uniform sensing layer,  $L$  has little effect on the sensing performance.

*Non-Uniform Sensing Layer*

The middle row of Fig. 5 and Table 5 describe the sensing performances of fiber-optic SPR sensors with non-uniform sensing layers of different  $k$ . The other sensor parameters are set as follows:  $T_m = 65$  nm,  $L = 10$  mm,  $\theta = 1.41 \sim \pi/2$ . The SPR dip has a little blue shift and its depth increases [see Fig. 5c], while  $S$  and  $Q$  slightly decrease with increasing  $k$  [see Fig. 5d and Table 5]. Thus, in the case of a non-uniform sensing layer (when  $L = 10$  mm),  $k$  also has little effect on the sensing performance.

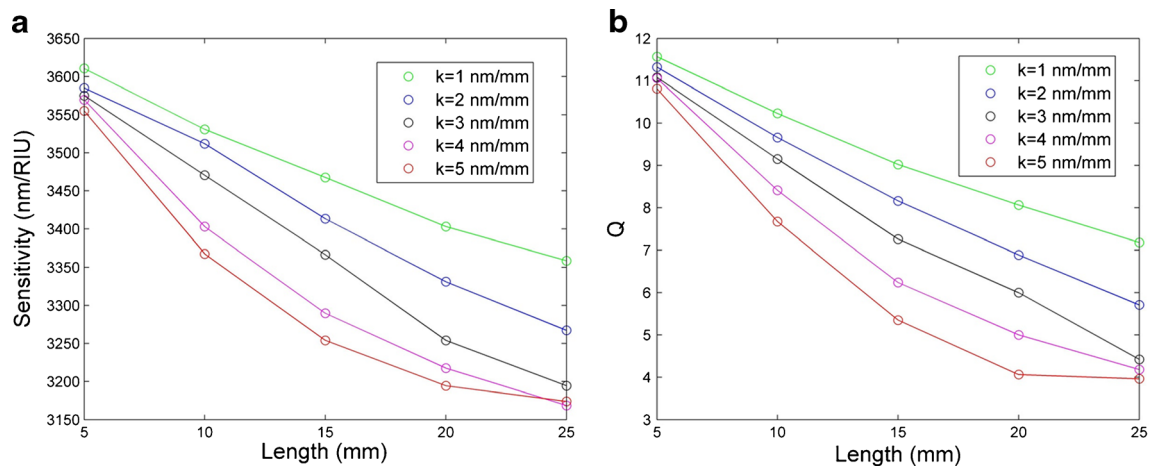


**Fig. 6** The relationship of sensitivity or  $Q$  and the length of sensing region by “ $1.41 \sim \pi/2$ ” multimode incident fiber-optic SPR sensors with different non-uniform sensing layers: **a** sensitivity; **b**  $Q$ . All the sensitivities and  $Q$ s are obtained at 1.35 RI surrounding

### Length of the Sensing Region with a Non-Uniform Sensing Layer

We further study fiber-optic SPR sensors with a non-uniform sensing layer and different  $L$ , as shown in the bottom row of Fig. 5 and Table 6. The other sensor parameters are set as follows:  $T_m = 65$  nm,  $k = 5$  nm/mm,  $\theta = 1.41 \sim \pi/2$ . From Fig. 5e, we can see that the SPR dip is strongly broadened with an increase of  $L$ , which results in a rapid decline in  $Q$  (described in detail in Table 6).  $S$  also has a more considerable reduction with increasing  $L$  compared to part “3.3.1.” Thus, in the case of a non-uniform sensing layer with  $k$  of 5 nm/mm,  $L$  has an obvious effect on the sensing performance.

Finally, we study the effect of  $L$  on fiber-optic SPR sensors with different non-uniform sensing layers (as described in Fig. 6).  $L$  has an increasing effect on  $S$  and  $Q$  as  $k$  increases.

## Conclusions

We have proposed a new fiber-optic SPR sensor model with a non-uniform sensing layer which can be set to satisfy different coating conditions. The effects of incident light modes and non-uniform sensing layers on the performances of fiber-optic SPR sensor are investigated. Results indicate that the higher order incident mode yields higher  $S$ , but lower  $Q$ . The optimal incident multimode form is selected as  $1.41 \sim \pi/2$ . The non-uniformity of the sensing layer has little effect on the sensing performances when  $L$  is 10 mm. However,  $L$  has an obvious effect on the sensing performances in the case of a non-uniform sensing layer. Moreover,  $L$  has an increasing effect on the sensing performances when  $k$  increases.

Our new model provides a simulation method that is much closer to the actual situation. Using our model, the distributions and non-uniformities of sensing layers can be set to satisfy different coating conditions. Additionally, the model can even be used to accurately study the performances of fiber-optic SPR sensor with various multilayers.

### Compliance with Ethical Standards

**Conflict of Interest** This work is jointly supported by the National Science Foundation of China under Grant Nos. of 61308046 and 61275125, Doctoral Fund of Ministry of Education of China (Nos. 20114408120002 and 20124408110003), and the Basic Research Program funds of Shenzhen. Corresponding authors the High-level Talents Project of Guangdong Province. The authors declare that they have no conflict of interest.

This chapter does not contain any studies with human participants or animals performed by any of the authors.

**Informed Consent** Informed consent was obtained from all individual participants included in the study.

## References

1. Yuan Y, Hu D, Hua L, Li M (2013) Theoretical investigations for surface plasmon resonance based optical fiber tip sensor. *Sensors Actuators B Chem* 188:757–760
2. Gupta G, Kondoh J (2007) Tuning and sensitivity enhancement of surface plasmon resonance sensor. *Sensors Actuators B Chem* 122(2):381–388
3. Sonny S, Sesay AM, Virtanen V (2010) Development of diagnostic SPR based biosensor for the detection of pharmaceutical compounds in saliva. *Proc SPIE* 7376:737605
4. Li YC, Chiou CC, Luo JD, Chen WJ, Su LC, Chang YF, Chang YS, Lai CS, Lee CC, Chou C (2012) Sensitive detection of



- unlabeled oligonucleotides using a paired surface plasma waves biosensor. *Biosens Bioelectron* 35(1):342–348
5. Xu LF, Vaidyanathan VG, Cho BP (2014) Real-time surface plasmon resonance study of biomolecular interactions between polymerase and bulky mutagenic DNA lesions. *Chem Res Toxicol* 27(10):1796–1807
  6. Jorgenson RC, Yee SS (1993) A fiber-optic chemical sensor based on surface plasmon resonance. *Sensors Actuators B Chem* 12(3): 213–220
  7. Kim SA, Kim SJ, Moon H, Jun SB (2012) In vivo optical neural recording using fiber-based surface plasmon resonance. *Opt Lett* 37(4):614–616
  8. Sharma NK, Rani M, Sajal V (2013) Surface plasmon resonance based fiber optic sensor with double resonance dips. *Sensors Actuators B Chem* 188:326–233
  9. Liu Z, Wei Y, Zhang Y, Zhang Y, Zhao E, Yang J, Yuan L (2015) Twin-core fiber SPR sensor. *Opt Lett* 40(12):2826–2829
  10. Nayak JK, Parhi P, Jha R (2015) Graphene oxide encapsulated gold nanoparticle based stable fibre optic sucrose sensor. *Sensors Actuators B Chem* 221:835–841
  11. Ghatak A, Thyagarajan K (1998) An introduction to fiber optics. Cambridge University Press, Cambridge, pp. 82–83
  12. Gupta BD, Sharma AK (2005) Sensitivity evaluation of a multi-layered surface plasmon resonance-based fiber optic sensor: a theoretical study. *Sensors Actuators B Chem* 107(1):40–46
  13. Homola J (1997) On the sensitivity of surface plasmon resonance sensors with spectral interrogation. *Sensors Actuators B Chem* 41: 207–211
  14. Tabassum R, Gupta BD (2015) Performance analysis of bimetallic layer with zinc oxide for SPR-based fiber optic sensor. *J Lightwave Technol* 33(22):4565–4571
  15. Wu J, Yan Y, Li S, Ding X, Ding S, Huang Y (2015) Monitoring of patient glucose infusion using a surface plasmon resonance-based fiber optic sensor. *Meas Sci Technol* 26:105701
  16. Tan ZX, Hao X, Li XJ, Chen YZ, Hong XM, Fan P (2016) Angular characteristics of a multimode fibre surface plasmon resonance sensor under wavelength interrogation. *J Phys D Appl Phys* 49:025401
  17. Li DC, Zhu R, Wu P, Pang K, Wu JW, Zeng ZM, Xu KX (2013) A distinguishing method of different petrol by fiber-optic surface plasmon resonance sensor. *Proc SPIE* 8621:86211N
  18. Sharma AK, Gupta BD (2004) Absorption-based fiber optic surface plasmon resonance sensor: a theoretical evaluation. *Sensors Actuators B Chem* 100(3):423–431
  19. Sharma AK, Jha R, Gupta BD (2007) Fiber-optic sensors based on surface plasmon resonance: a comprehensive review. *IEEE Sensors J* 7(8):1118–1129
  20. Chen YZ, Yu YQ, Li XJ, Zhou HS, Hong XM, Geng YF (2016) Fiber-optic urine specific gravity sensor based on surface plasmon resonance. *Sensors Actuators B Chem* 226:412–418
  21. Sharma AK, Mohr GJ (2008) On the performance of surface plasmon resonance based fibre optic sensor with different bimetallic nanoparticle alloy combinations. *J Phys D Appl Phys* 41:055106
  22. Chen YZ, Yu YQ, Li XJ, Tan ZX, Geng YF (2015) Experimental comparison of fiber-optic surface plasmon resonance sensors with multi metal layers and single silver or gold layer. *Plasmonics* 10(6): 1801–1808